https://doi.org/10.17221/142/2018-SWR

Soil water response to rainfall in a dune-interdune landscape in Horqin Sand Land, northern China

Xueya Zhou[1,2], Dexin Guan[2], Jiabing Wu[2], Fenghui Yuan[2], Anzhi Wang[2], Cangjie Jin[2], Yushu Zhang[3]*

[1]*Key Laboratory of Geospatial Technology for the Middle and Lower Yellow River Regions, Ministry of Education, College of Environment and Planning, Henan University, Kaifeng, P.R. China*
[2]*Key Laboratory of Forest Ecology and Management, Institute of Applied Ecology, Chinese Academy of Sciences, Shenyang, P.R. China*
[3]*Institute of Atmospheric Environment, China Meteorological Administration, Shenyang, P.R. China*
**Corresponding author: waz@iae.ac.cn*

Citation: Zhou X., Guan D., Wu J., Yuan F., Wang A., Jin C., Zhang Y. (2019): Soil water response to rainfall in a dune-interdune landscape in Horqin Sand Land, northern China. Soil & Water Res., 14: 229–239.

Abstract: Soil water dynamic is considered an important process for water resource and plantation management in Horqin Sand Land, northern China. In this study, soil water content simulated by the SWMS-2D model was used to systematically analyse soil water dynamics and explore the relationship between soil water and rainfall among micro-landforms (i.e., top, upslope, midslope, toeslope, and bottomland) and 0–200 cm soil depths during the growing season of 2013 and 2015. The results showed that soil water dynamics in 0–20 cm depths were closely linked to rainfall patterns, whereas soil water content in 20–80 cm depths illustrated a slight decline in addition to fluctuations caused by rainfall. At the top position, the soil water content in different ranges of depths (20–40 and 80–200 cm) was near the wilting point, and hence some branches, and even entire plants exhibited diebacks. At the upslope or midslope positions, the soil water content in 20–80 or 80–200 cm depths was higher than at the top position. Soil water content was higher at the toeslope and bottomland positions than at other micro-landforms, and deep caliche layers had a positive feedback effect on shrub establishment. Soil water recharge by rainfall was closely related to rainfall intensity and micro-landforms. Only rainfalls > 20 mm significantly increased water content in > 40 cm soil depths, but deeper water recharge occurred at the toeslope position. A linear equation was fitted to the relationship between soil water and antecedent rainfall, and the slopes and R^2 of the equations were different among micro-landforms and soil depths. The linear equations generally fitted well in 0–20 and 20–40 cm depths at the top, upslope, midslope, and toeslope positions (R^2 value of about 0.60), with soil water in 0–20 cm depths showing greater responses to rainfall (average slope of 0.189). In 20–40 cm depths, the response was larger at the toeslope position, with a slope of 0.137. In 40–80 cm depths, a good linear fit with a slope of 0.041 was only recorded at the toeslope position. This study provides a soil water basis for ecological restoration in similar regions.

Keywords: antecedent rainfall; micro-landforms; response magnitude; soil water dynamics

Soil water plays a pivotal role in land-atmosphere interactions, including rainfall infiltration, runoff generation, and groundwater recharge (Puri *et al.* 2011). In arid and semi-arid ecosystems, soil water availability is the principal factor limiting the number and size of perennial plant species, thus exerting the main constraint regarding vegetation restoration and permanent desertification control

Supported by the National Basic Research Program of China (2013CB429902); Zhongyuan Scholarship Program, China (182101510005); and Key Projects of the Chinese Academy of Sciences (KFZD-SW-305).

https://doi.org/10.17221/142/2018-SWR

(Jian *et al*. 2015). Natural precipitation is the main source of soil water and groundwater recharge, and largely affects the temporal and spatial heterogeneity of soil water (Wilson *et al*. 2004) and water budgets at both local and catchment scales (Tweed *et al*. 2011). Many studies have addressed the roles of rainfall characteristics (Liu *et al.* 2016), terrain (Svetlitchnyi *et al*. 2003), and vegetation types (Schlueter *et al*. 2013) in soil water dynamics in arid and semiarid areas. For example, in arid and semiarid environments, Kurc and Small (2007) indicated that rainfall of < 5 mm returned to the atmosphere through evapotranspiration, whereas large rainfall events (> 5 mm) could wet the rooting zone of shrubs beyond the depth of evaporative demand. Schade and Hobbie (2005) found that woody plants altered the spatial and temporal distributions of soil water content through rainfall interception and shading of the soil surface. Scott *et al.* (2008) demonstrated that uptake and hydraulic redistribution by roots might further alter the water distribution in soils.

Horqin Sandy Land is located in the semiarid agro-pastoral transition zone between the Inner Mongolian Plateau and the Northeast Plains of China and has become one of the most severely desertified regions due to long-term human disturbances such as overgrazing and extensive firewood gathering (Zhu & Chen 1994). The Horqin Sandy Land grassland ecosystems are typically sensitive to climate changes and fragile to human activities (Zhang *et al*. 2012). The degradation of these grasslands is related to the mobility of the sandy soils and is divided into four categories, including fixed, semi-fixed, semi-shifting, and shifting sandy lands. Dune-interdune is the main landscape pattern of Horqin Sandy Land. Since the 1980s, *Caragana microphylla*, a dominant plant species, has been gradually planted to stabilize sand dunes with the help of straw checkerboards (Cao *et al*. 2011). Some sand-fixing shrubs thrive in early growth stages; however, with increasing age, these plantations have exhibited diebacks in some areas. A plausible explanation is an imbalance between water supply and plant demands, with water shortage regarded as the main limitation for the growth of sand-fixing shrubs (Li *et al*. 2004). Climate change, particularly a decrease in precipitation and subsequent frequency of droughts, may exacerbate the consequences of the imbalance between soil water supply and plants water consumption.

The relationship between soil water and precipitation has become one of the most important areas of research for hydrologic studies and restoration of degraded ecosystems in Horqin Sandy Land (Liu *et al*. 2016). Wei *et al*. (2013) noted that micro-topography (dune position and elevation) promotes differences in soil water conditions and causes differences in plant growth. Despite the obvious importance of these processes in determining the effectiveness of efforts to slow down or reverse desertification, few studies have quantitatively addressed soil water dynamics and their responses to rainfall characteristics at micro-landform scales in dune-interdune areas. Field experiments are time-consuming, costly, and site-specific, and thus numerical modelling methods are widely used to predict the soil water distribution under various conditions (Šimůnek *et al*. 2008). The HYDRUS commercial modelling software has been widely adopted to predict soil water movement (Kandelous & Šimůnek 2010). Furthermore, SWMS, another popular simulation tool, is simpler than HYDRUS for modelling soil water distribution (Gribb & Sewell 1998). Thomas *et al*. (2008) applied SWMS to investigate the hillslope hydrological mechanisms related to the management of water resources in north-western France. For its flexibility and reliability, SWMS was selected for the simulation of soil water distribution in this study.

This research was based on the simulation of soil water content (SWC) by the SWMS-2D model. The objectives were to explore SWC variations occurring within various micro-landforms, soil depths, rainfall patterns, and vegetation characteristics. Furthermore, the response of soil water to rainfall patterns was investigated. The results of this work should bring new insights into the hydrology of degraded ecosystems in semi-arid dune-interdune habitats.

MATERIAL AND METHODS

Study site and data. The study site is located in western Horqin Sandy Land, northeastern Inner Mongolia, China (42°41'–45°15'N, 118°35'–123°30'E, and 498 m a.s.l.), a region with a semiarid continental monsoon climate. The annual mean rainfall is 284 mm, with about 70% of this falling between June and August. The annual mean potential evapotranspiration is over 2300 mm. The annual average temperature is 6.2°C, with a minimum monthly mean temperature of –11.7°C in January and a maximum of 23.6°C in July. The prevailing wind direction is northwest in winter and spring, and southwest to south in summer and autumn. The mean annual

https://doi.org/10.17221/142/2018-SWR

wind velocity is 4.2 m/s. Dunes, alternating with gently undulating interdune lowlands, characterize the landscape in this region. The vegetation is dominated by shrubs such as *C. microphylla* in the dunes, and *Tamarix chinensis* or *Salix flavida* in the lowlands. Some herbaceous plants, including *Leymus chinensis*, *Setaria viridis*, *Bassia dasyphylla*, among others, are randomly dispersed under these shrubs. The groundwater table of the dune is deeper than 5 m, which is beyond root water uptake. Precipitation is usually the only water source for vegetation.

A typical area of dune-interdune was selected as the experiment plot. In this area, a *C. microphylla* plantation was planted in 1 × 1 m^2 straw checkerboard sand barriers in the 1980s. The experimental site was enclosed after planting. A transect (~90 m) was projected on the southeast-northwest direction of the plot, crossing from the dune´s top to the bottomland (Figure 1). The sampling of soil was performed at 5–10 m intervals along the experimental transect using 3 repetitions. The elevation of the sample positions was measured using a Global Positioning System (GPS) device and a geometric gradient. At each sample position, soil samples were taken with a soil corer (diameter of 8 cm) at 10 cm increments from the surface to a depth of 200 cm (3 repetitions at each depth) and sealed in order to be shipped to the lab. The SWC of the samples was measured by the oven-dry method. Volumetric SWC was obtained by converting gravimetric SWC through soil bulk density (BD). Sampling was repeated about every ten days from 26 April to 16 September during 2013 and 2015. The investigation of the vegetation was performed in five micro-landforms during mid-to-late August 2015. Three random quadrats of 5 × 5 m^2 were set up in each micro-landform, resulting in a total of 15 quadrats. In each quadrat, the height, number of branches and canopy size of shrubs, and vegetation cover were measured and recorded. The daily rainfall data were obtained from a meteorological station located about 1000 m from the study area.

Soil water simulations. The SWMS-2D model was employed to simulate water movement in the experimental field (Šimůnek *et al.* 1994). Using a Galerkin linear finite element method, the code numerically solves the two-dimensional form of the Richards' equation:

$$\frac{\partial \theta}{\partial t} = \frac{\partial}{\partial x_i}\left[K(h)\left(K_{ij}^{A}\frac{\partial h}{\partial x_j} + K_{iz}^{A} \right)\right] - S \quad (1)$$

where:

θ – volumetric water content (L^3/L^3)

t –is the time (T)

h – pressure head (L)

x_j – spatial coordinates (i =1, 2)

$K(h)$ – unsaturated hydraulic conductivity (L/T)

S – sink or source term (/T)

K_{ij}^{A} – components of a dimensionless anisotropy tensor

A two-dimensional flow domain in the x–z plane was considered (Figure 1). The domain was 90 m long and 1.4–11.5 m deep (about 490 m^2), with a network of triangular and quadrilateral elements (about 1613) created. Relatively small elements with 5 cm grid spacing were used near the soil surface or the vertically capillary zone. Between them, the size of the elements increased with depth to reflect slower changes in pressure heads owing to less environmental impacts at these depths. Five soil types were defined within the flow domain (Figure 1) and soil main physical properties are presented in Table 1. Soil hydraulic properties (SHPs) were described

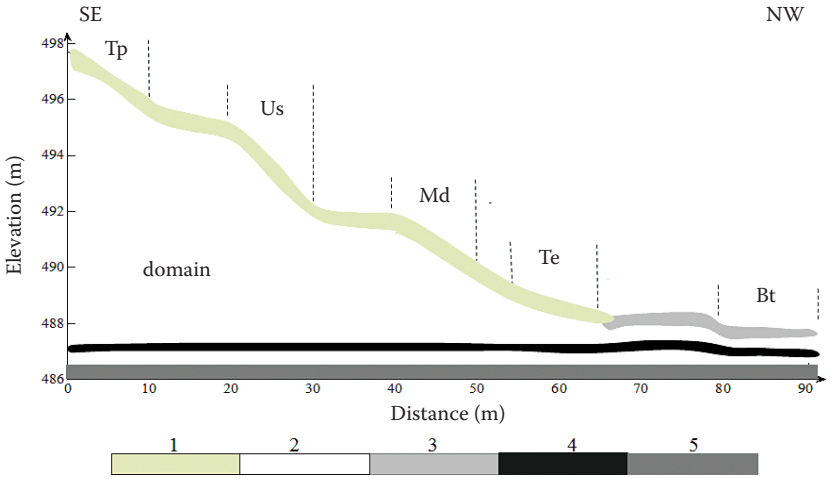

Figure 1. Schematic side view of the studied slope with distinct soil horizons

1–5 represent different soil types; Tp, Us, Md, Te, and Bt represent the top, upslope, midslope, toeslope, and bottomland positions

https://doi.org/10.17221/142/2018-SWR

Table 1. Soil physical properties and calibrated hydraulic parameters

Soil type	1	2	3	4	5
Sand (%)	93 ± 2	98 ± 1	75 ± 15	72 ± 6	94 ± 3
Clay (%)	7 ± 2	2 ± 1	25 ± 15	28 ± 6	6 ± 3
Organic matter (%)	0.10 ± 0.01	0.05 ± 0.01	3.61 ± 0.21	8.02 ± 0.34	0.06 ± 0.01
Bulk density (g/cm^3)	1.55 ± 0.01	1.57 ± 0.01	1.47 ± 0.05	1.50 ± 0.01	1.56 ±0.01
θ_s (cm^3/cm^3)	0.38	0.33	0.5	0.5	0.35
θ_r (cm^3/cm^3)	0.001	0.001	0.01	0.01	0.01
K_s (cm/d)	40	65	5	4	20
n	1.6024	2.0024	1.2074	1.3024	1.2524
α (/cm)	0.015	0.0195	0.025	0.0229	0.023

θ_s, θ_r – saturated and residual water contents; K_s – saturated hydraulic conductivity; α, n –parameters controlling the shape of the retention curve

by the Van Genuchten-Mualem (VG) model in the SWMS-2D code (Van Genuchten 1980), whose initial prediction was performed using pedotransfer functions and soil textural information (Schaap & Leij 1998). During calibration, SHPs were adjusted by assessing the simulated and measured SWC values presenting minimum bias (Table 1). The VG model included soil water retention $\theta(h)$ and hydraulic conductivity $K(h)$, which were represented as follows:

$$\theta(h) = \begin{cases} \theta_r + \dfrac{\theta_s - \theta_r}{\left[1 + |\alpha h|^n\right]^m}, & h < 0 \\ \theta_s, & h \geq 0 \end{cases} \quad (2)$$

$$K(h) = \begin{cases} K_s S_e^l \left[1 - \left(1 - S_e^{1/m}\right)^m\right], & h < 0 \\ K_s, & h \geq 0 \end{cases} \quad (3)$$

where:

$$S_e = \frac{\theta(h) - \theta_r}{\theta_s - \theta_r} = \left[1 + \left(|\alpha h|^n\right)\right]^{-m} \quad (4)$$

$$m = 1 - 1/n,\ n > 1 \quad (5)$$

where:

S_e – effective water content

θ_s, θ_r – saturated and residual water contents (L^3/L^3)

K_s – saturated hydraulic conductivity (L/T)

α (/L), n – parameters controlling the shape of the retention curve

l – pore connectivity and tortuosity factor, which is often set as 0.5

The pressure head was estimated from the VG model and SWC measured on 26 April 2013 and 2015, and its initial (t = 0) distribution was determined by the interpolation of measurements. The boundary conditions varied daily during simulations. The upper boundary conditions were defined from rainfall and potential evapotranspiration (PET) data calculated according to the Penman-Monteith equation (Allen *et al*. 1998). The bottom boundary was set as variable flux boundary conditions. No flux boundary conditions were prescribed on the left and right sides. The initial calculation time step was 0.01 days and the minimum time step was 0.0001 days.

Root water uptake $S(h,x,z)$ was described by the Feddes approach (Feddes *et al*. 1976), which calculates the spatial distribution of root-water uptake as a function of potential water uptake rate $S_p(x,z)$ and water stress response $a(h)$. The spatial distribution of potential water uptake rate was defined by assigning a root-distribution function $b(x, z)$ to each node (Vogel & Cislerova 1988), implemented according to root density and depth obtained by field observations and literature (Niu *et al*. 2013).

$$S(h,x,z) = \alpha(h) S_p(x,z) \quad (6)$$

$$S_p(x,z) = b(x,z) L_t T_p \quad (7)$$

where:

T_p – potential transpiration rate (L/T)

L_t – width (L) of the soil surface associated with the transpiration process

Data analyses. In this paper, we utilized the SWMS-2D model (Šimůnek *et al*. 1994) to analyse SWC dynamics and their responses to rainfall. The root mean square error (RMSE) between measured and simulated SWC was used to assess model performance, which was represented as follows:

https://doi.org/10.17221/142/2018-SWR

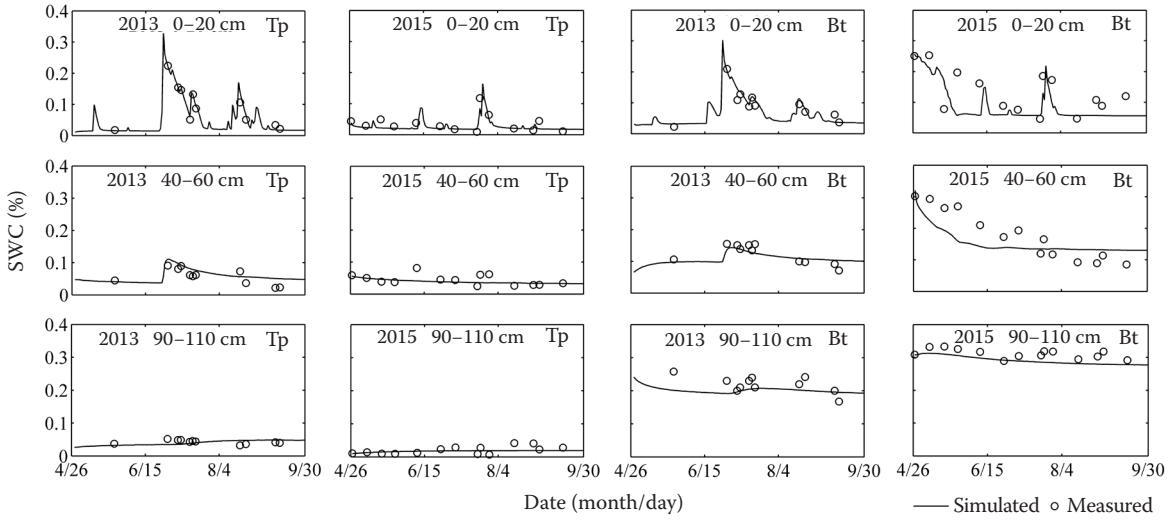

Figure 2. Temporal dynamics of simulated versus measured soil water content (SWC) at different micro-landforms and depths in 2013 and 2015 (Tp and Bt represent the top and bottomland positions, respectively)

$$RMSE = \left[\frac{1}{N} \sum_{i=1}^{N} \left(S_i - M_i \right)^2 \right]^{\frac{1}{2}} \quad (8)$$

where:

S_i – simulated SWC (cm^3/cm^3)

M_i – measured SWC (cm^3/cm^3)

N – number of observations

Five micro-landforms, including the top (0–10 m), upslope (20–30 m), midslope (40–50 m), toeslope (55–65 m), and bottomland (80–90 m) were selected as analytic targets (Figure 2). The soil water content of the corresponding micro-landforms was calculated by averaging the SWC for a depth interval within the corresponding length interval (e.g., 0–10 m) of the slope. Statistical analysis of shrub growth characteristics was performed using SPSS 13.0 (SPSS Inc., USA).

The response of soil water to rainfall events was analysed by selecting four events with different rainfall intensities during the study period, which included: event 1 (5.4 mm on 6 June 2013), event 2 (15.3 mm on 10 May 2015), event 3 (24.9 mm on 24 July 2015), and event 4 (60 mm on 26 June 2013). The linear equations were fitted to the relationship between SWC and antecedent cumulative rainfall (prophase 1–30 days). The relationship was quantified by analysing and comparing the slope and determination coefficient (R^2).

RESULTS

SWC dynamics among micro-landforms

The SWMS-2D model was validated for the SWC of the study area with an RMSE of about 0.02 cm^3/cm^3 (Figure 2, Zhou *et al*. 2017), which indicated a good model performance.

The simulated SWC data indicated that SWC in 0–20 cm depths sharply fluctuated with rainfall (Figure 3). In the 20–40 cm and 40–80 cm depths, especially at the bottomland position, SWC generally had a slight decline in the whole growing season except for a SWC increase occurring after rainfalls > 10 mm. Addition-

Table 2. Growth characteristics of sand-binding shrubs during the growing season

Location	Mean cover (%)	Mean canopy size (cm × cm)	Mean height (cm)	Mean branches (No. per plant)
Tp	32.8 ± 1.7[a]	(72.1 ± 2.1) × (62.3 ± 1.9)[a]	69.7 ± 2.1[a]	7 ± 2[a]
Us	31.9 ± 1.5[a]	(79.4 ± 3.1) × (72.6 ± 2.8)[b]	86.7 ± 3.8[b]	9 ± 3[b]
Md	43.5 ± 2.1[b]	(78.1 ± 3.5) × (72.2 ± 2.2)[b]	84.3 ± 3.6[b]	9 ± 2[b]
Te	57.2 ± 6.2[c]	(107.2 ± 5.5) × (92.0 ± 4.3)[c]	117.8 ± 4.7[c]	11 ± 4[c]
Bt	83.0 ± 10.3[d]	(210 ± 3.8) × (212.5 ± 3.0)[d]	272.5 ± 3.4[d]	30 ± 6[d]

Letters a, b, c, and d indicate significant differences between micro-landforms at $P < 0.05$; Tp, Us, Md, Te, and Bt represent the top, upslope, midslope, toeslope, and bottomland positions

https://doi.org/10.17221/142/2018-SWR

ally, the SWC increases in 20 to 40 cm depths were larger than those in 40–80 cm depths after rainfall.

Furthermore, SWC dynamics (Figure 3) and plants responses (Table 2) were different among micro-landforms. At the top position, although mean SWC in 40–80 cm depths was 0.045 cm^3/cm^3, SWC in the 20–40 and 80–200 cm depths was near to or lower than the wilting humidity (0.025 cm^3/cm^3; Figure 3Tp). Therefore, the plants grew poorly and exhibited die-backs of some branches or entire plants. At the upslope position, SWC was relatively higher, especially in 20–40 cm and 40–80 cm depths (root zone), and the averages were 0.042 and 0.054 cm^3/cm^3, respectively (Figure 3Md). The height, canopy size, and number of branches were significantly greater than those at the top position. At the midslope position, although SWC in 20–80 cm depths was low, SWC in 80–200 cm depths was above the wilting humidity and far higher than that at the top and upslope positions (Figure 3Us), which led to robust plant growth. At the toeslope and bottomland positions, SWC was higher than at other positions, with SWC up to 0.4 cm^3/cm^3 (Figure 3Bt, Te) around 130 and 90 cm depths in toeslope and bottomland positions, respectively. The highest SWC at the bottomland position led to the greatest plants cover, height, and number of branches. Additionally, bottomland SWC reductions were abundant from the beginning to the end of the growing season, with SWC in the 20–40 and 40–80 cm depths decreasing by 0.20 and 0.13 cm^3/cm^3, respectively (Figure 3Te).

Response of SWC to rainfall patterns

Rainfall patterns. Total rainfall amount was 242 and 157.6 mm during the growing season in 2013 and 2015, respectively, and 55.7 and 24.4% of those were contributed by rainfall events of > 10 mm, respectively (Table 3). Daily rainfall greater than 20 mm occurred on 26 June 2013 (60 mm) and 24 July 2015 (24.9 mm), accounting for 24.8 and 15.8% of total rainfall, respectively. A total of 45 rainfall events occurred in 2013 and 47 in 2015, with 68.9 and 76.6% of the contributing less than 5 mm, 17.8 and 19.1% between 5 and 10 mm, 11.1 and 2.1% between 10 and 20 mm, and 2.2 and 2.1% more than 20 mm, respectively. The maximum interval between rain events was 13 days in 2013 and 16 days in 2015.

Response of SWC to rainfall events. Based on rainfall patterns in the study area, we selected four rainfall events with different intensities to assess the response of the simulated SWC to rainfall (Figure 4). Infiltration depth and SWC were strongly associated with rainfall intensity. Overall, a rainfall of 8.9 mm influenced the SWC only in 0–10 cm depths, letting the rainwater quickly evaporate back into the atmosphere within 24 h. Rainfall of 15.3 mm caused certain

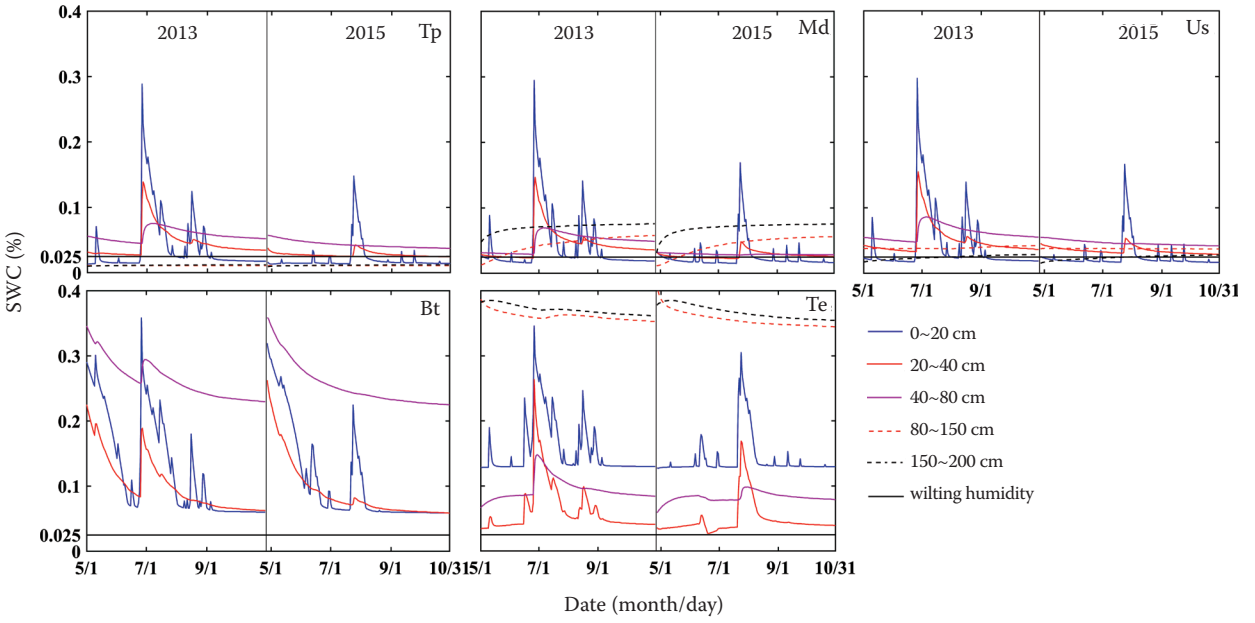

Figure 3. Soil water content (SWC) dynamics simulated by the SWMS-2D model at different micro-landforms during the growing season of 2013 and 2015 (Tp, Us, Md, Te, and Bt represent the top, upslope, midslope, toeslope, and bottomland positions, respectively)

https://doi.org/10.17221/142/2018-SWR

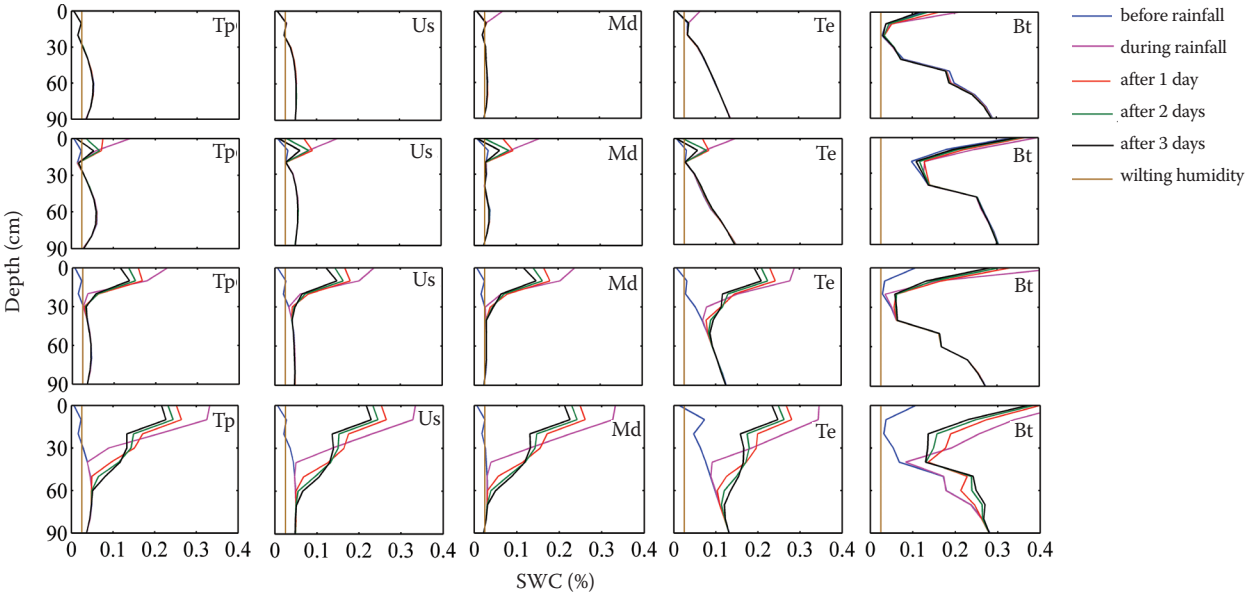

Figure 4. Changes in simulated soil water content (SWC) as a result of rainwater infiltration into the soil under rainfall events of, from top to bottom, 8.9, 15.3, 24.9, and 60 mm (Tp, Us, Md, Te, and Bt represent rainwater infiltration at the top, upslope, midslope, toeslope, and bottomland positions, respectively)

replenishment of SWC in 0–40 cm depths, while rainfall of 24.9 mm made a prominent SWC increase within 0–60 cm depths. When rainfall reached 60 mm (the heaviest rainfall during the experimental period), SWC significantly increased in 0–80 cm depths.

The micro-topography variations resulted in differences in rainwater infiltration, with slight differences occurring at the top, upslope, and midslope positions; however, apparent differences were observed at the toeslope and bottomland positions (Figure 4). After rainfalls of 15.3 mm, the maximum infiltration depth at the top, upslope, midslope, and toeslope positions was 20 cm less than that at the bottomland position. Rainfall events with 24.9 mm provided some recharge to a depth of 60 cm at the toeslope position, about 20 cm more than that at the top, upslope, midslope, and bottomland positions. Under rainfalls of 60 mm, rainwater reached a depth of 80 cm at the toeslope or bottomland positions, which was about 10 cm more than that at the top, upslope, and midslope positions.

Change of SWC as a function of the cumulative rainfall. Based on the response of SWC to the rainfall events mentioned above, rainfall minimally influenced SWC below 80 cm depth among microlandforms. The linear fits were accurate to describe

Table 3. Rainfall characteristics during the growing season

Year	Rainfall intensity (mm/day)	Frequency distribution (times)	Percentage of frequency (%)	Rainfall amount (mm)	Percentage of rainfall (%)
2013	0–5	31	68.9	54.4	22.4
	5–10	8	17.8	52.9	21.9
	10–20	5	11.1	74.7	30.9
	> 20	1	2.2	60	24.8
	total	45	100	242	100
2015	0–5	36	76.6	54.5	34.6
	5–10	9	19.1	64.6	41
	10–20	1	2.1	13.6	8.6
	> 20	1	2.1	24.9	15.8
	total	49	100	157.6	100

https://doi.org/10.17221/142/2018-SWR

the empirical relations between the simulated SWC and 1–30 days of antecedent rainfall in 0–20, 20–40, and 40–80 cm depths. The slopes, intercepts, and R^2 of the linear equations are presented in Figure 5. The larger the slope was, the bigger the response magnitude of soil water to rainfall was.

Linear relationships between SWC and antecedent rainfall varied among micro-landforms and soil depths. The linear equations generally fitted well in the 0–20 cm and 20–40 cm depths among micro-landforms except for the bottomland position (R^2 was about 0.20), with the average R^2 being 0.613 and 0.568, respectively. In these linear fits, the optimal fitting models were between SWC and 12 and 18 days of antecedent rainfall for the 0–20 cm and 20–40 cm depths, respectively. In 40–80 cm depths, a linear relationship only existed at the toeslope position, and R^2 was greater than 0.60 between SWC and 23–30 days of antecedent rainfall. Finally, R^2 at the bottomland position, regardless of depth, was less than 0.2, implying a weak linear relationship between SWC and rainfall.

The response magnitude of soil water to antecedent rainfall decreased with increasing depth, with averages of the slopes being 0.189, 0.088, and 0.030 for the 0–20 cm, 20–40 cm, and 40–80 cm depths, respectively. In 0–20 cm depths, the response of soil water to daily rainfall was larger than to antecedent rainfall, with a slope of about 0.435. In 20–40 cm depths, although SWC barely showed a response to daily rainfall, SWC was linearly correlated with antecedent cumulative rainfall and averages of the slopes were 0.057–0.137 among micro-landforms, of which mean slope at the toeslope position (0.137) was greater than those at the top, upslope, and midslope positions (0.058, 0.059, and 0.056, respectively). In 40–80 cm depths, the slope was 0.041 at the toeslope position.

DISCUSSION

Dynamics of SWC. In the semi-arid dune-interdune landscape, SWC was simulated with soil hydraulic parameters estimated from soil textural information and effectively adjusted to fit the measurements. Overall, the model performance was good, with RMSE of about 0.02 cm^3/cm^3. Based on the simulation results, SWC was highly variable over space and time. The heterogeneity of SWC is primarily ascribed to rainfall, topography, soil depth, soil texture, and vegetation. Among micro-landforms, superficial soil water (< 20 cm depth) was subject to dramatic variations resulting from rainfall infiltration and soil evaporation. The amplitude of soil water fluctuations was damped with increased soil depth, which was similar to the findings of Wu *et al*. (2002). Between the top and midslope positions, surface SWC was generally similar but less than that of the toeslope and

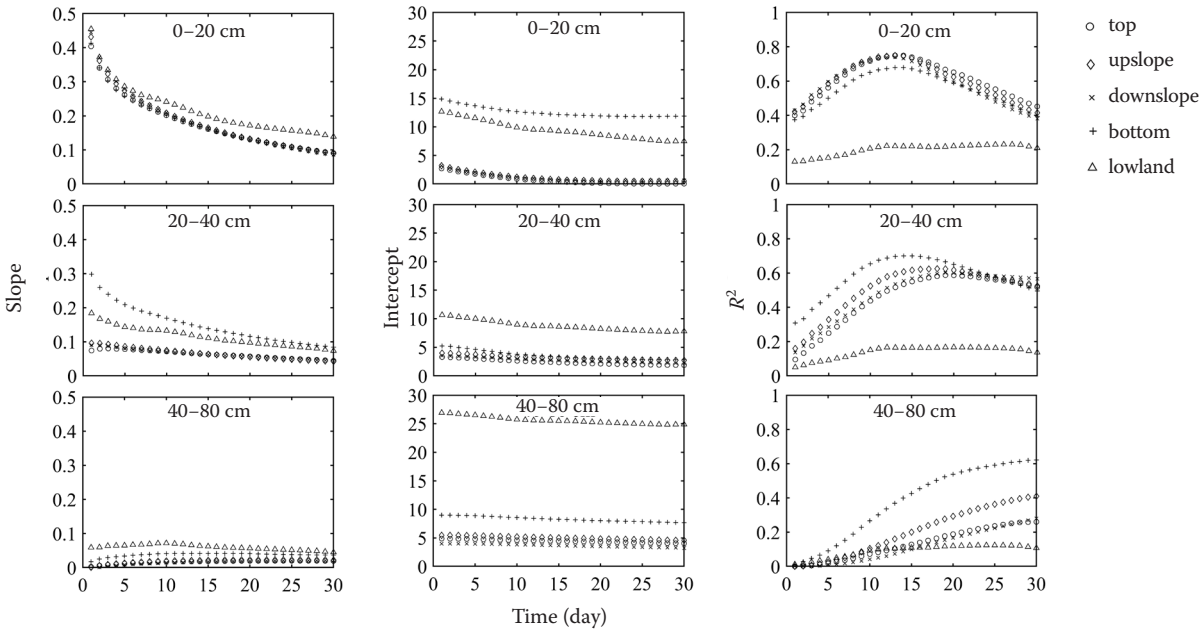

Figure 5. Changes in slope, intercept, and R^2 of the linear equations between simulated soil water content (SWC) and 1–30 days of antecedent rainfall at different micro-landforms and depths

https://doi.org/10.17221/142/2018-SWR

bottomland positions. This difference was primarily attributed to lower hydraulic conductivity and higher water holding capacity at the toeslope and bottomland positions (Table 1). Bottomland SWC showed a lower soil water pulse, presumably due to higher canopy interception rainfall and less soil evaporation. In > 20 cm depths, SWC responded differently at varying soil depths and micro-landforms, showing larger spatial variability. At the top position, SWC was almost equal to or less than the wilting humidity. This soil water condition would restrain plant growth. At the upslope and midslope positions, the higher SWC in the roots zone or deeper soil led to appropriate plant growth. At the toeslope and bottomland positions, soil water was higher, with the highest SWC in the bottomland position leading to the best plant growth state and maximum soil water consumption. Additionally, calcic horizons are very common in semiarid dune-interdunes, having very low hydraulic conductivity (Hennessy *et al*. 1983) which could serve as 'dams' to store water in wet periods and release water for plants during drought periods. In our study, calcic horizons appeared in the toeslope, at ~130 cm, and bottomland, at ~90 cm depths (soil type 4 in Figure 1), resulting in high SWC and forming a beneficial self-adaptive mechanism for shrub survival in drought periods.

Response of soil water to rainfall patterns. Rainfall is the main water source for ecosystems in the study area and regulates soil water variation during the growing season. Rainfall events between 5 and 10 mm played a minor role in replenishing soil water, whereas rainfall events between 10 and 20 mm generally had a greater impact on upper soil (0–40 cm) and only rainfalls larger than 20 mm provided some recharge to the deeper soil (> 40 cm). This result is consistent with the results of Yao *et al*. (2013), Yang *et al*. (2017), and He *et al*. (2012), who suggested that the significant response depth of soil water after rainfalls of < 20 mm was 0–40 cm. In our study, after rainfall, SWC decreased rapidly in 0–20 cm depths during the first day, primarily because of the large soil hydraulic conductivity. During the second and third days after rainfall, there was soil water downward transport for 24.9 mm and 60 mm rainfall events, but not for a 15.3 mm rainfall, which meant that larger rainfalls could cause longer and deeper percolation. This might be related to larger hydraulic conductivity and lower saturated water content in deeper soil than in upper soil. Zhang *et al*. (2018) obtained similar findings by simulating soil water distribution after irrigation in a semiarid area. Similarly, Cable and Huxman (2004) found that, in water-limited ecosystems, the effects of small rainfall events on soil water might persist for just a few hours. In the same ecosystem, Schwinning and Sala (2004) indicated that the influence of larger rainfall events on soil water could extend deeper into the soil and persist for several days. Nevertheless, previous work did not systematically study the effect of micro-landforms on rainfall recharge possesses. Topography was the dominant factor in soil water distribution (Brocca *et al*. 2009). Our study showed that when rainfall was less than 20 mm, maximum recharge depth at the toeslope position was similar to that at the top, upslope, and midslope positions; whereas in rainfalls under >20 mm, soil water recharge depth was larger at the toeslope position. This could be explained by water budget differences, with high-intensity rainfalls producing horizontal movement of soil water towards the toeslope and bottomland positions with larger plant cover and increasing the extent and depth of soil water recharge (Thomas *et al*. 2008; Li *et al*. 2013), and small rainfall events causing little surface runoff (Zhou *et al*. 2017). Additionally, hydraulic properties differences controlled the infiltration characteristics and rainfall recharge depth of soil among micro-landforms (Zhai & Rahardjo 2015).

The effective antecedent rainfall makes a great contribution to SWC, which includes the prophase rainfall and current rainfall (Wei *et al*. 2005). Linear or curve fittings were generally used to explore the mathematical relationship between SWC and antecedent rainfall. For example, Wei *et al.* (2005) used linear equations to better describe the relationship between SWC and rainfall, while Jia *et al*. (2016) fitted the relationship with quadratic equations. In our study, a linear fitting, which depended on micro-landforms and depths, between SWC and rainfall was better. Among micro-landforms, except for the bottomland position, the determination coefficient between SWC in the 0–20 cm and 20–40 cm depths and 1–30 days of antecedent rainfall was 0.613 and 0.568, respectively, showing good fit. The optimal fitted models were between SWC and 12 or 18 days of antecedent rainfall. In 40–80 cm depths, the linear model between SWC and 23–30 days of antecedent rainfall fitted well only at the toeslope position, with a determination coefficient > 0.600. However, SWC at the bottomland position, regardless of depth, presented a weak linear relationship with rainfall, which was mainly due to the involvement of groundwater in the water cycle within the soil layer. The dependence of SWC on antecedent rainfall decreased with increasing depth. This conclusion is consistent with the results of previous studies (Wei *et al*. 2005; Jia *et al*. 2016), which

https://doi.org/10.17221/142/2018-SWR

emphasized that surficial soil water exhibited the highest correlation with rainfall. The response magnitude of surface SWC to current rainfall was larger than to antecedent rainfall, and deep SWC response to antecedent rainfall was larger at the toeslope position than at the top, upslope, and midslope positions. Therefore, in a semiarid dune-interdune landscape, antecedent cumulative rainfall is important to recharge root-zone water, especially at the toeslope position.

CONCLUSIONS

Based on the results simulated by the SWMS-2D model, the main conclusions can be smmarized as follows:

Soil water dynamics were linked to rainfall patterns, micro-landforms, soil depths, soil texture, and vegetation characteristics. Soil water in 0–20 cm depths was closely related to rainfall patterns and displayed prominent but different temporal fluctuations among micro-landforms. In 20–80 cm depths, soil water content displayed a slight decline during the growing season but increased after rainfalls > 10 mm. At the top, upslope, or midslope positions, soil water content was generally low and, particularly at the top position, SWC in different range of depths (e.g., 20–40 and 80–200 cm depths) was near to or lower than the wilting humidity. At the toeslope and bottomland positions, soil water content was higher and deep caliche layers had a positive feedback effect on shrub establishment.

Soil water recharge by rainfall was closely related to rainfall intensity and micro-landforms. Only rainfalls > 20 mm significantly increased water content below 40 cm in depth among micro-landforms, but deeper water recharge occurred only at the toeslope position. The linear equations were better for the interpretation of the relationship between soil water and rainfall, which varied among micro-landforms and soil depths. For 0–20 cm or 20–40 cm soil depths, the linear equations generally fitted well except for the bottomland position. Soil water in 0–20 cm depths exhibited the highest correlation with rainfall, with an average slope of 0.189, and soil water response magnitude to current rainfall was larger than prophase rainfall. In 20–40 cm depths, soil water response magnitude to prophase rainfall was larger at the toeslope position, with a slope of 0.137. For 40–80 cm soil depths, only the toeslope position showed a good linear fit, whose slope was 0.041.

Acknowledgements. We thank to A. Musa, Y. Luo, T. Yang, and H. Wang for their valuable help with field work.

References

Allen R.G., Pereira L.S., Raes D., Smith M. (1998): Crop Evapotranspiration – Guidelines for Computing Crop Water Requirements. FAO Irrigation and Drainage Paper 56, Rome, FAO.

Brocca L., Melone F., Moramarco T., Morbidelli R. (2009): Soil moisture temporal stability over experimental areas in Central Italy. Geoderma, 148: 364–374.

Cable J.M., Huxman T.E. (2004): Precipitation pulse size effect on Sonoran Desert soil microbial crusts. Oecologia, 141: 317–324.

Cao C.Y., Jiang S.Y., Ying Z., Zhang F.X., Han X.S. (2011): Spatial variability of soil nutrients and microbiological properties after the establishment of leguminous shrub *Caragana microphylla* Lam. plantation on sand dune in the Horqin Sandy Land of Northeast China. Ecological Engineering, 37: 1467–1475.

Feddes R.A., Kowalik P., Kolinskamalinka K., Zaradny H. (1976): Simulation of field water-uptake by plants using a soil-water dependent root extraction function. Journal of Hydrology, 31: 13–26.

Gribb M.M., Sewell G. (1998): Solution of ground water flow problems with general purpose and special purpose computer codes. Ground Water, 36: 366–372.

He Z.B., Zhao W.Z., Liu H., Chang X.X. (2012): The response of soil moisture to rainfall event size in subalpine grassland and meadows in a semi-arid mountain range: A case study in northwestern China's Qilian Mountains. Journal of Hydrology, 420: 183–190.

Hennessy J.T., Gibbens R.P., Tromble J.M., Cardenas M. (1983): Water properties of caliche. Journal of Range Management, 36: 723–726.

Jia D.Y., Wen J., Zhang T.T., Xi J.J. (2016): Responses of soil moisture and thermal conductivity to precipitation in the mesa of the Loess Plateau. Environmental Earth Sciences, 75: 395.

Jian S.Q., Zhao C.Y., Fang S.M., Yu K. (2015): Effects of different vegetation restoration on soil water storage and water balance in the Chinese Loess Plateau. Agricultural and Forest Meteorology, 206: 85–96.

Kandelous M.M., Šimůnek J. (2010): Numerical simulations of water movement in a subsurface drip irrigation system under field and laboratory conditions using HYDRUS-2D. Agricultural Water Management, 97: 1070–1076.

Kurc S.A., Small E.E. (2007): Soil moisture variations and ecosystem-scale fluxes of water and carbon in semiarid grassland and shrubland. Water Resources Research, 43: 1–13.

Li X.R., Ma F.Y., Xiao H.L., Wang X.P., Kim K.C. (2004): Long-term effects of revegetation on soil water content of sand dunes in arid region of Northern China. Journal of Arid Environments, 57: 1–16.

https://doi.org/10.17221/142/2018-SWR

Li X.Y., Zhang S.Y., Peng H.Y., Hu X., Ma Y.J. (2013): Soil water and temperature dynamics in shrub-encroached grasslands and climatic implications: Results from Inner Mongolia steppe ecosystem of north China. Agricultural and Forest Meteorology, 171: 20–30.

Liu X.P., He Y.H., Zhao X.Y., Zhang T.H., Li Y.L., Yun J.Y., Wei S.L., Yue X.F. (2016): The response of soil water and deep percolation under *Caragana microphylla* to rainfall in the Horqin Sand Land, northern China. Catena, 139: 82–91.

Niu C.Y., Musa A., Zong Q., Luo Y.M., Toshio O., Sun G.F., Liu Q. (2013): Allocation patterns of above-and below-ground biomass of *Caragana microphylla* in Horqin Sandy Land, north China. Chinese Journal of Ecology, 32: 1980–1986. (in Chinese, English abstract)

Puri S., Stephen H., Ahmad S. (2011): Relating TRMM precipitation radar land surface backscatter response to soil moisture in the Southern United States. Journal of Hydrology, 402: 115–125.

Schaap M.G., Leij F.J. (1998): Database-related accuracy and uncertainty of pedotransfer functions. Soil Science, 163: 765–779.

Schade J.D., Hobbie S.E. (2005): Spatial and temporal variation in islands of fertility in the Sonoran Desert. Biogeochemistry, 73: 541–543.

Schlueter S., Vogel H.J., Ippisch O., Vanderborght J. (2013): Combined impact of soil heterogeneity and vegetation type on the annual water balance at the field scale. Vadose Zone Journal, 12: 1–17.

Schwinning S., Sala O.E. (2004): Hierarchy of responses to resource pulses in and and semi-arid ecosystems. Oecologia, 141: 211–220.

Scott R.L., Cable W.L., Hultine K.R. (2008): The ecohydrologic significance of hydraulic redistribution in a semiarid savanna. Water Resources Research, 44: 1–12.

Šimůnek J., Vogel T., Van Genuchten M.T. (1994): The SWMS-2D Code for Simulating Water Flow and Solute Transport in Two-dimensional Variably Saturated Media (Version 1.21), Research Report No. 132, U.S. Salinity Laboratory Agricultural Research Service, Riverside, USDA.

Šimůnek J., Van Genuchten M.T., Šejna M. (2008): Development and applications of the HYDRUS and STANMOD software packages and related codes. Vadose Zone Journal, 7: 587–600.

Svetlitchnyi A.A., Plotnitskiy S.V., Stepovaya O.Y. (2003): Spatial distribution of soil water content within catchments and its modeling on the basis of topographic data. Journal of Hydrology, 277: 50–60.

Thomas Z., Molenat J., Caubel V., Grimaldi C., Merot P. (2008): Simulating soil-water movement under a hedgerow surrounding a bottomland reveals the importance of transpiration in water balance. Hydrological Processes, 22: 577–585.

Tweed S., Leblanc M., Cartwright I., Favreau G., Leduc C. (2011): Arid zone groundwater recharge and salinisation processes; an example from the Lake Eyre Basin, Australia. Journal of Hydrology, 408: 257–275.

Van Genuchten M.T. (1980): A closed-form equation for predicting the hydraulic conductivity of unsaturated soils. Soil Science Society of America Journal, 44: 892–898.

Vogel T., Cislerova M. (1988): On the reliability of unsaturated hydraulic conductivity calculated from the moisture retention curve. Transport in Porous Media, 3: 1–15.

Wei Y.F., Fang J., Liu S., Zhao X.Y., Li S.G. (2013): Stable isotopic observation of water use sources of *Pinus sylvestris* var. *mongolica* in Horqin Sandy Land, China. Trees-structure and Function, 27: 1249–1260.

Wei Z.G., Wen J., Lv S.H. (2005): A primary field experiment of land–atmosphere interaction over the loess plateau and its ground surface energy in clear day. Plateau Meteorology, 24: 545–555. (in Chinese with English abstract)

Wilson D.J., Western A.W., Grayson R.B. (2004): Identifying and quantifying sources of variability in temporal and spatial soil moisture observations. Water Resources Research, 40: 1–10.

Wu W., Geller M.A., Dickinson R.E. (2002): The response of soil moisture to long-term variability of precipitation. Journal of Hydrometeorology, 3: 604–613.

Yang J.J., He Z.B., Du J., Chen L.F., Zhu X., Lin P.F., Li J. (2017): Soil water variability as a function of precipitation, temperature, and vegetation: a case study in the semiarid mountain region of China. Environmental Earth Sciences, 76: 206.

Yao S.X., Zhao C.C., Zhang T.H., Liu X.P. (2013): Response of the soil water content of mobile dunes to precipitation patterns in Inner Mongolia, northern China. Journal of Arid Environments, 97: 92–98.

Zhai Q., Rahardjo H. (2015): Estimation of permeability function from the soil-water characteristic curve. Engineering Geology, 199: 148–156.

Zhang G.L., Don J.W., Xiao X.M., Hu Z.M., Sheldon S. (2012): Effectiveness of ecological restoration projects in Horqin Sandy Land, China based on SPOT-VGT NDVI data. Ecological Engineering, 38: 20–29.

Zhang Y.L., Feng S.Y., Wang X.F., Binley A. (2018): Simulation of soil water flow and heat transport in drip irrigated potato field with raised beds and full plastic-film mulch in a semiarid area. Agricultural Water Management, 209: 178–187.

Zhou X.Y., Guan D.X., Wu J.B., Yang T.T., Yuan F.H., Musa A., Jin C.J., Wang A.Z., Zhang Y.S. (2017): Quantitative investigations of water balances of a dune–interdune landscape during the growing season in the Horqin sandy land, Northeastern China. Sustainability, 9: 1–13.

Zhu Z.D., Chen G.T. (1994): Sandy Desertification in China. Beijing, Science Press.

Received for publication July 1, 2018
Accepted after corrections March 11, 2019
Published online April 10, 2019